C. R. Mecanique 343 (2015) 1–12

Contents lists available at ScienceDirect

Comptes Rendus Mecanique

www.sciencedirect.com

Design of a device to induce swirling flow in pipes: A rational approach

François Beaubert [a], Halldór Pálsson [b], Sylvain Lalot [a,*], Isabelle Choquet [c], Hadrien Bauduin [a]

[a] TEMPO, UVHC, Campus Mont Houy, 59313 Valenciennes cedex 9, France
[b] University of Iceland, Sæmundargötu 2, 101 Reykjavik, Iceland
[c] University West, Department of Engineering Science, 46186 Trollhättan, Sweden

ARTICLE INFO

Article history:
Received 7 March 2014
Accepted 4 September 2014
Available online 16 October 2014

Keywords:
Computational fluid dynamics
Laminar
Decay
Swirl
Bézier
OpenFOAM

ABSTRACT

In this study, a rational approach is proposed to design a device for inducing swirling flow in heat exchanger pipes, for improved efficiency in the laminar regime. First, 2D computational fluid dynamics results lead to select, among four profiles, the blade profile with the most favorable lift to drag ratio. Then, the fluid flow in the swirler made with the selected blade profile is simulated in 3D, for Reynolds numbers ranging from 50 to 1600. Based on the simulation results, an analytic approximation of the evolution of the tangential fluid velocity is proposed as a function of the Reynolds number.

1. Introduction

Heat exchangers are used in many types of applications with the aim of transferring heat from one fluid to the other in an efficient manner. The shell and tube type heat exchangers are among the most common heat exchangers. In most cases, the fluid flowing inside the pipes of these kinds of heat exchangers is in the turbulent regime, since it provides heat transfer rates much higher than in the laminar regime (see, e.g., [1]). However, there are some specific applications where laminar flow can be expected, for example when the working fluids are highly viscous or when the transporting pipe diameter is small. Consequently, low heat transfer rate and increased fouling rate occur.

Different methods for increasing heat transfer in laminar and mildly turbulent flows in tubes have been investigated for years. One particular technique leading to wall shear stress enhancement is to induce rotating or swirling flows inside the pipe. Swirling flows in circular or annular tubes have been widely investigated for the turbulent regime [2–4] but less for the laminar regime [5–7]. These flows are formed supplementing the axial velocity with a tangential velocity component, turning the flow either clockwise or counter-clockwise and giving it a helical motion, or the so-called corkscrew pattern. One of the most widely used methods consists in installing helical spirals or other fins, either inside or outside heat exchanger tubes [8–10]. This method greatly enhances heat transfer and, since it increases the wall shear stress, the fouling rate is also globally reduced. But the drawbacks of such an installation are a really high increase in pressure drop and the presence of local fouling in areas close to the fins where low velocities can be expected. It also may complicate cleaning procedures.

* Corresponding author. Tel.: +33 327 511 973; fax: +33 327 511 961.
E-mail address: sylvain.lalot@univ-valenciennes.fr (S. Lalot).

http://dx.doi.org/10.1016/j.crme.2014.09.004
1631-0721/

Confined swirling flows can be classified into two main categories: the first one is the continuous swirling flow, for which the swirl pattern is quite constant along the pipe. The second category is the decaying swirling flow. Most continuous swirling flows are produced by inserting full-length twisted-tapes or helical screw tapes into the pipes [11,12]. Such a way to induce swirling flows is particularly efficient in increasing heat transfer, but it usually generates a too large pressure drop, which is a drawback. This is even worse if an inner rod is installed to hold the tapes on location, which is equivalent to an annular tube configuration. Swirl can also be driven by an axially rotating pipe wall [13]. This technique is mainly used for fundamental investigations and validation of numerical models developed to predict swirling flows.

For decaying swirling flows, the flow which is axial is given an additional angular component at a specific cross section, usually at the inlet of the tubes. The helical movement continues along the pipe for a certain distance, but residual swirl effects might still be visible after a considerable greater distance [14]. One advantage of inducing the swirl motion at a single cross section is that a large portion of the downstream pipe volume is free of any inserted objects that could trap deposits (local fouling) or a hindrance when cleaning the tubes.

Decaying swirling flows can be generated by rotating a section of the pipe, by using tangential injectors [15,16], or by the use of a so-called swirl inducing device, whose appellation in the literature can slightly differ. Among others, the names are: swirling device, swirler device or even shorter: swirler. Various swirler types exist and their applicability can be forced rotating, freely rotating, or fixed (static), to name a few. Forced swirlers, as for example rotating honeycombs, must be avoided in tubular heat exchangers because of excessive pressure drop, power consumption and installation costs. For the purposes of swirling flows in heat exchangers, they should be considered as a source of flow structure information. Static swirlers in circular tubes can be short-length twisted tapes, short twisted-fins or axial guide vanes [17–19].

Two main conclusions can be drawn from the already cited works. Firstly, studies of the profiles of the radial component of the velocity show that it does not play an important role in the evolution and decay of the swirling motion. Secondly, the main contribution to the swirl is related to the tangential component of the velocity. The tangential velocity field can generally be divided into three regions: i) the core region near the axial centerline where the tangential velocity is proportional to the radius, as in a forced vortex; ii) the annular region, where a free vortex occurs and the tangential velocity is inversely proportional to the radius—note that at the intersection of the first two regions, the tangential velocity reaches a maximum; iii) the wall region, which corresponds to a boundary layer. A swirling flow can thus be considered as a combined vortex. The maximum of the tangential velocity decays in the axial downstream direction and the position of this maximum moves towards the center line. So the size of the core region decreases along the axis.

In most studies dealing with short static swirlers, the effect of the variation of different parameters such as the twist angle of the blades, the number of blades, the distance between blades or the length of the blades are presented. To the authors' knowledge no study presents the swirler design process as is done in [20] or [21] for turbine blades; the focus of this paper is the presentation of such a process. It should however be added that a static swirler does not exactly resemble a turbine, nor a compressor, but rather something in between, since no mechanical energy is involved when the fluid flows through the swirler. This design process is three-fold and is followed in the present study. The first step is the selection of a 2D profile, based on the lift-to-drag ratio of the blades. The second step is the computation of 3D flow fields in the domain affected by the swirling flow. The last step is the determination of the Reynolds number range for which the assumption made in the first step is valid. Thus, in the first part of this paper, a blade design process is presented, which is based on hydrodynamic considerations in order to get a desired tangential velocity profile. The second part of the paper presents the resulting flow properties that are obtained using Computational Fluid Dynamics (CFD), for Reynolds numbers in the range 50 to 1600, ensuring a laminar flow regime. The latter is based on the tube diameter and on the mean axial velocity upstream the swirler.

2. The blade design

A general design concern of a swirler is to maximize the swirling effect of the internal flow in a tube, without increasing pressure drop excessively. Two sources of pressure drop are most important here: i) friction because of insertion of blades (hydrofoils). ii) The disturbance of the otherwise smooth flow profiles in a low Reynolds number tube flow. The first source can be related to the number of blades chosen and to their thickness, as well as the structure of the swirler (e.g., how blades are connected). The second source is related to the blade shape and how well they direct the flow into a smooth swirling motion, preferably without generating local vortices. Fig. 1 shows an example of a static swirler having eight blades.

The purpose of the blades is to force the fluid to deviate from its initial direction. This deviation, which represents the amount of swirling in the tube, is defined by the so-called "flow exit angle" ϕ. Fig. 2 shows the definition of the parameters that define the shape of the blades in this study. The blades have zero thickness and are therefore only defined by the camber line shape. Note that as the paper focuses on the geometrical definition of the swirler, it is more adapted to define the swirler in terms of geometrical parameters than to define the swirler in terms of fluid dynamics parameters such as the swirl number.

The blade exit angle θ, at a given radial location determined by a diameter D, differs from the actual flow exit angle ϕ of the velocity by a deviation angle δ due to the fact that the fluid will not "follow" the blade profile exactly. A rule of thumb is

$$\delta = m\frac{(90-\theta)}{\sigma^n}$$

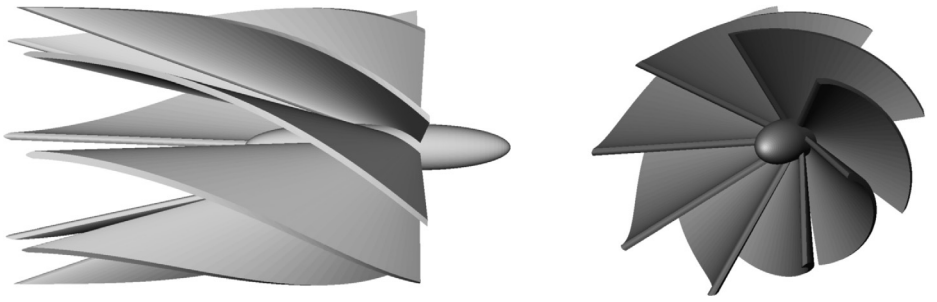

(fluid flows from left to right) (front view)

Fig. 1. Example of an eight-blade swirler.

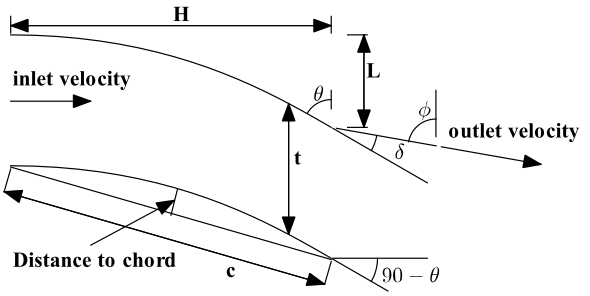

Fig. 2. Blade parameters.

where both angles (θ and δ) are given in degrees and $\sigma = c/t$ is the ratio between the chord length and the distance between blades, also called the solidity. In this study σ is constant, since a fixed diameter D has been chosen. The coefficient n is different between turbines and compressors, but as mentioned before, the swirler is neither a turbine nor a compressor and thus $n = 1/2$ is chosen arbitrarily here. The other coefficient m depends on several parameters such as the shape of the blade and the stagger angle, but in the current study a value of $m = 0.26$ is used which is recommended in [22].

To keep the solidity constant, the length of the blade varies with the radial location. The chord is $c = \sqrt{H^2 + L^2}$ and the distance between two blades is $t = \pi D/n_b$, where D is the diameter and n_b is the number of blades. It has to be noted that this rule is valid for standard turbine geometries where the radius is quite large with respect to the radial width of the flow channel. Hence, for swirlers studied in this paper and shown in Fig. 1, the deviation could be much different towards the axis of the flow.

It is well-known that there is no direct link between the performance of a 2D blade and its 3D counterpart when the height of the blades is not small compared to the hub radius due to 3D effects; see, e.g., the conclusion of [23]. In fact, in that case, the flow exit angle close to the hub observed in 3D is quite far from the flow exit angle determined in a 2D computation. So, among the infinite possible shapes for the blades, it has been decided to limit the present study to four different definitions of blade profiles. They are all based on the following constraints: i) the blade must be tangent to the axial flow at the inlet of the swirler. ii) The flow exit angle has to be respected for all radial locations. Note that for the application here, the blade exit angle is arbitrarily set to 48°, δ is set to 4°.

- The simplest profile studied here is defined by the linear variation of the tangent of the angle $90 - \theta$.
- The second profile is described by a polynomial that is constrained to give correct values of the tangent as well as zeros curvature at both extremities of the blade.
- The third profile is a Bézier curve (see, e.g., [24]) defined by the tangent at both extremities and a null curvature at the outlet extremity.
- The fourth profile is a Bézier curve defined by the tangent at both extremities and a null curvature at both extremities.

All these profiles are based on a given height H, which is linked to L by the first profile equation: $H = 2L\tan(\theta)$. It results in $c = L\sqrt{4\tan^2(\theta) + 1}$. By using the definitions of the various swirler parameters, it is found that the length L is determined by

$$L = \frac{\pi D}{n_b}\left(m\frac{90-\theta}{\delta}\right)^{\frac{1}{n}}\frac{1}{\sqrt{4\tan(\theta)+1}}$$

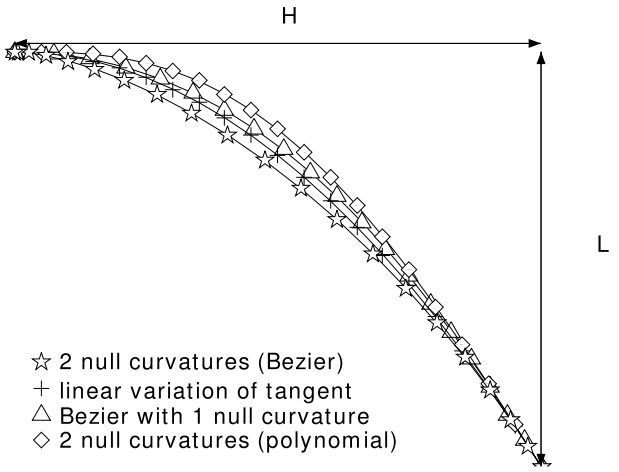

Fig. 3. Comparison of the four profiles.

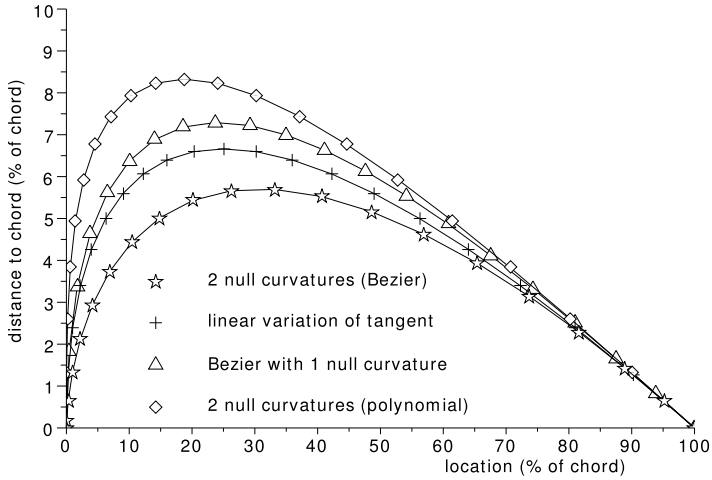

Fig. 4. Distance to the chord for the four profiles.

It can be concluded that L is linearly proportional to D, and consequently the height H also. Although the profiles look similar (see an example in Fig. 3), the distance to the chord (which is an important design parameter for turbine blades) is quite different (Fig. 4). Note that the maximum distance to the chord for the fourth profile is about one third of chord length from the leading edge, which is common for turbine blades.

The ratio of the lift coefficient to the drag coefficient (the lift-drag ratio) is considered to be the best criterion to select the profile that will be used to build the whole swirler. It depends on the distance between two blades, thus on the number of blades (Fig. 6). It is computed in 2D using CFD and the results are shown after a standard mesh sensitivity study based on the radial distribution of the velocity profile. Fig. 5 shows a schematic of the computational domain. The finest mesh consisted of around 10700 cells and the flow was laminar in all cases. The numerical study has been carried out using `simpleFOAM` as a solver, which is part of the OpenFOAM version 2.0.1 package [25,26]. It is a Finite-Volume Method-based solver [27,28], using a standard SIMPLE iteration scheme for solving the Navier–Stokes equations for incompressible fluids, in the steady state, with first-order upwind for the convection terms and second-order linear scheme for the diffusion, as often used in the literature for laminar flows, e.g., [29]. Note that the local Péclet number is higher than 2 for all Reynolds number considered in the present study. These schemes assure good convergence: the final residuals for the velocity, the pressure, and the continuity are of the order of magnitude of 10^{-11}.

It can be seen in Fig. 6 that for a blade exit angle lower than 65°, the most efficient profile is defined by a Bézier curve having a null curvature at both ends. For this profile, Fig. 7 shows that the ratio of the drag coefficient for four or six blades to the drag coefficient for eight blades does not depend on the blade exit angle if it is lower than 65°.

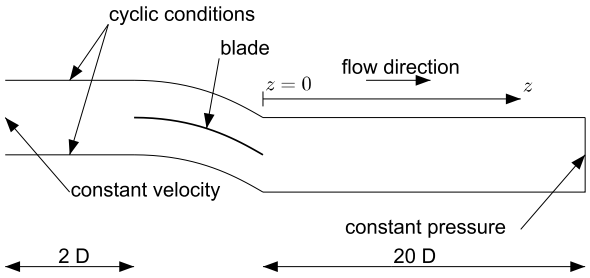

Fig. 5. Schematic of the 2D computational domain with the associated boundary conditions.

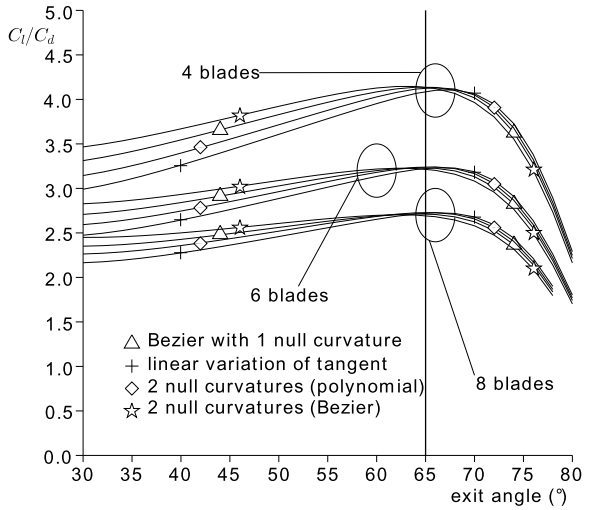

Fig. 6. Ratio of lift to drag coefficients.

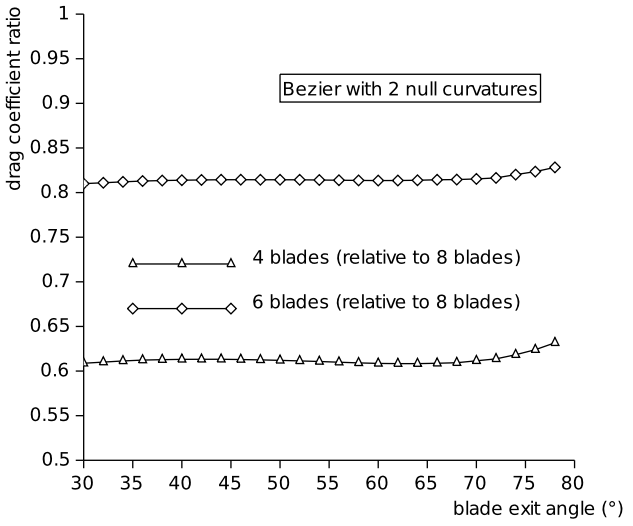

Fig. 7. Drag coefficient ratios when comparing four- and six-blade designs with an eight-blade design.

It is furthermore of relevance to study the energy dissipation of the different blade setups. This is shown in Fig. 8 in terms of a total pressure coefficient defined by

$$C_p = \frac{\dot{m}}{\frac{1}{2}\bar{u}^2} \int_A \left(p + \rho \frac{u^2}{2} \right) u_z \, \mathrm{d}A$$

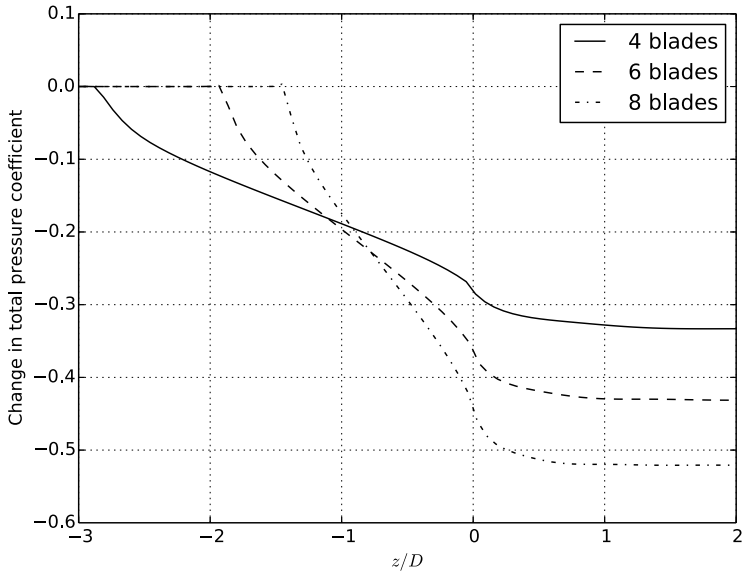

Fig. 8. Total pressure coefficient for the three different numbers of blades.

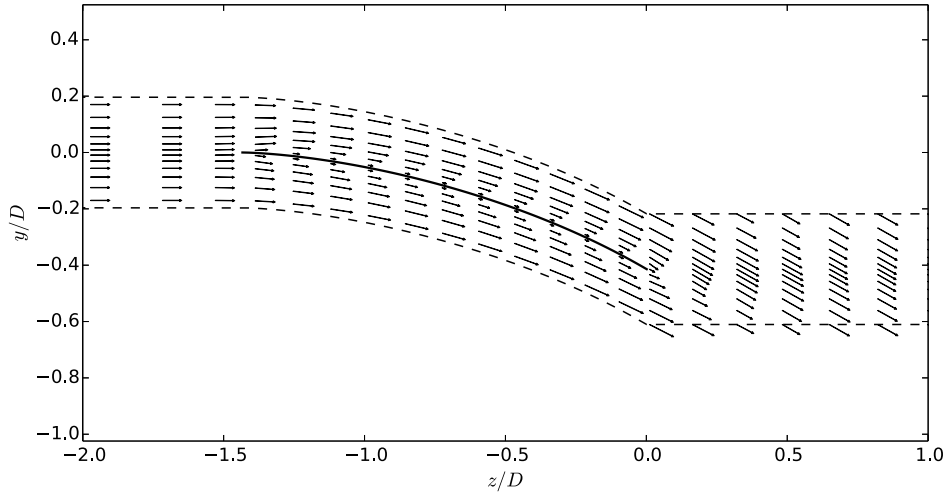

Fig. 9. Flow direction in two dimensions for an eight-blade setup using profile 4.

where A is the cross section area of the channel, $\dot{m}$ the mass flow, p the local pressure and u the velocity (with $\bar{u}$ denoting the average velocity in a channel). The figure clearly shows that the losses increase with increasing blade numbers, even though the four-blade swirler is longer, as seen in the final pressure drop at the blade exit. Finally, Fig. 9 shows the direction of the flow in the computational domain, going on either side of a single blade. It is clear that there is no reversed flow present and the velocity profile stabilizes quickly at the exit and becomes uniform.

Fig. 7 shows that the drag coefficient ratio for four blades is the lowest when compared to the eight-blade setup. Hence, it can be concluded that it is preferable to use four blades if the head loss is the main criterion. However, it can be argued that in order to obtain a better control of the flow (minimizing the risk of secondary flows) a swirler with higher solidity should be chosen, which would shift the preference to an increased number of blades.

3. Three dimensional flow field calculation

To verify that the desired effect of the swirler is achieved, a numerical study has been carried out using the same solver as described for the two-dimensional case. This is only done for the eight-blade design, since it can be argued that there is less fundamental difference between the 2D and 3D cases when the angle between individual blades is smaller. In a first step, two-dimensional lateral surfaces are generated in the OFF format, using Scilab [30] to produce the files. The 3D structured mesh is then constructed using a modified version of the `extrudeMesh` utility provided as a part of OpenFOAM,

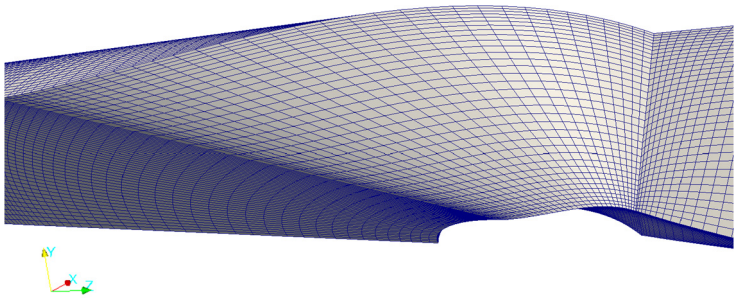

Fig. 10. Detailed view of the mesh (blade part).

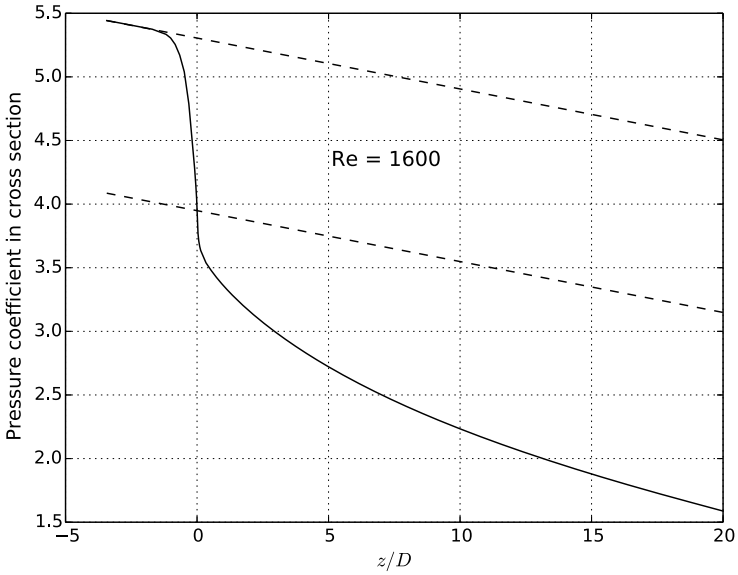

Fig. 11. Total pressure coefficient (solid line), with a comparison with standard pressure decay in laminar tube flow (dashed lines).

which rotates the 2D mesh around the swirler axis. After a standard mesh sensitivity study, based on radial velocity profiles, the final mesh consists of around 800,000 hexahedral cells (except on the axis of the tube). Mesh quality criteria such as skewness, mesh non-orthogonality, and edge ratio are in a good agreement with the constraints required by OpenFOAM. Fig. 10 shows a detailed view of the mesh that includes the swirler blades.

At the inlet of the computational domain (two diameters upstream of the swirler) a standard parabolic velocity profile is imposed. The computational domain extends 20 diameters downstream from the swirler outlet section, as shown in Fig. 5. At the outlet of the domain, a constant static pressure is imposed as well as zero gradients for the velocity. A non-slip boundary condition is applied to the wall of the pipe, on the swirler blades, and on the swirler inner core. Cyclic boundary conditions are applied to all other boundaries.

Fig. 11 shows the evolution of the total pressure coefficient along the pipe axis for a Reynolds number of 1600. The rapid head loss in the swirler corresponds to a loss coefficient of 1.4. It is furthermore interesting to study the flow structure near the exit of the swirler in order to verify its effect. Fig. 12 shows the results at two locations as normalized components in cylindrical coordinates, namely $U_z/\bar{U}_z$, $U_r/\bar{U}_z$ and $U_\theta/\bar{U}_z$. An asymmetrical effect is clearly seen in all the figures at the swirler exit (Fig. 12-left), but it has almost disappeared at $z/D = 1$ (Fig. 12-right). A substantial amount of radial flow is present at the exit, thus indicating strong secondary flow. In spite of the secondary flow at the exit, these effects seem to disappear quickly and, at $z/D = 1$, the flow is predominantly in a swirling mode with a laminar boundary layer forming on the pipe wall, but still rather low velocity near the center.

As mentioned before, the main goal of the study is to know if the flow exit angle in the range $48° \pm 4°$ is obtained over the entire domain at the outlet of the swirler. Figs. 13 and 14 show the flow exit angle distribution at $z/D = 0$ and the "swirling" angle at $z/D = 1$. The swirling angle is computed as the flow exit angle in any cross section. Note that these figures confirm that the discrepancy between 2D computations and 3D results for the flow exit angle is the largest close to the hub.

Fig. 15 shows that the mass flow averaged exit angle $\overline{\phi} = \frac{\sum(\dot{m}\phi)_{\text{cell}}}{\dot{m}_{\text{total}}}$ (see Fig. 2) at the outlet of the swirler varies from 57° to 51°, for a Reynolds number varying from 50 to 1600. It also shows that to keep the mean flow exit angle within the

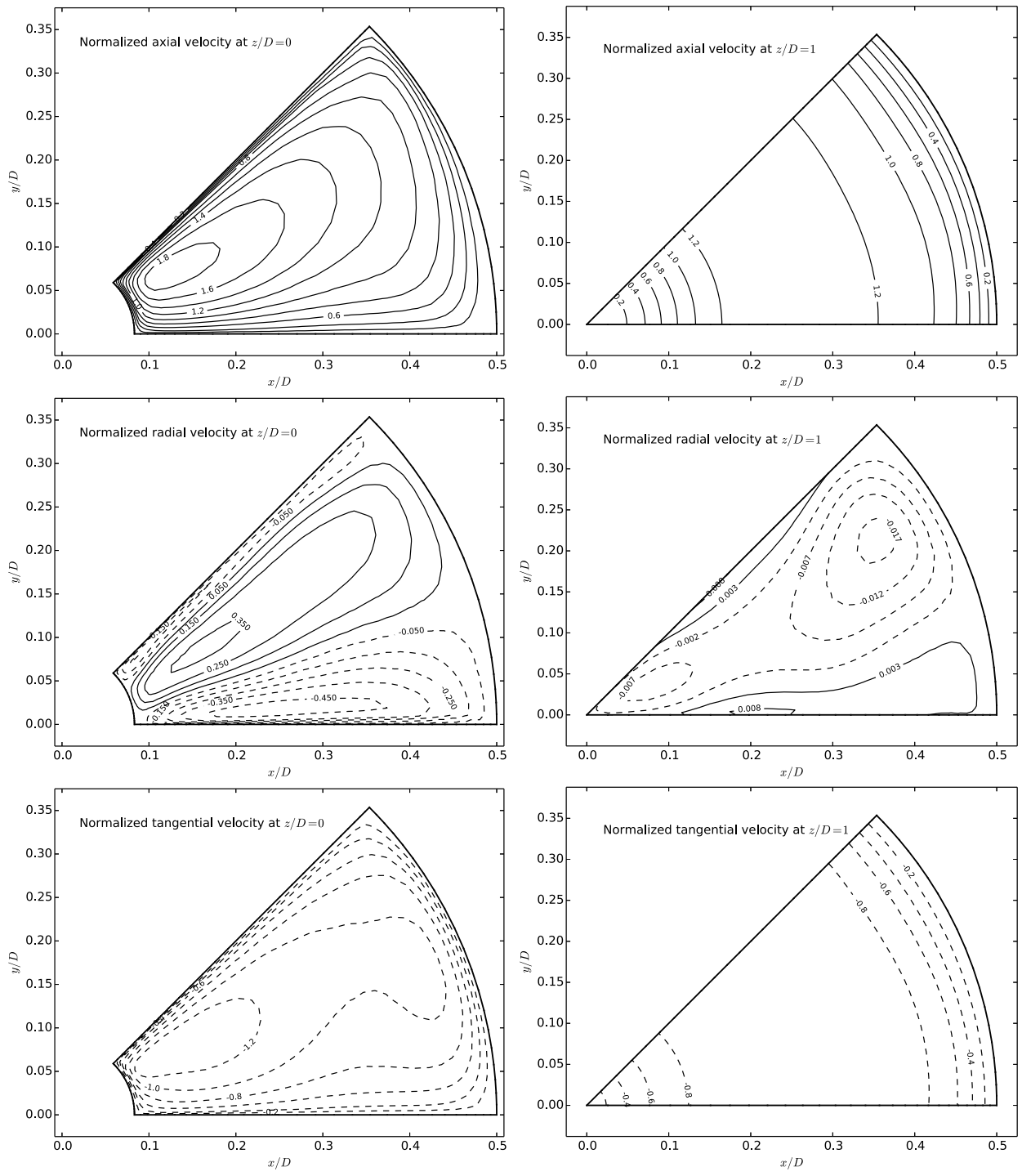

Fig. 12. Normalized flow velocity with respect to the average axial speed in the pipe, for axial flow (top), radial flow (middle) and tangential flow (bottom). The velocities are shown at the swirler exit (left) and one diameter downstream of the exit (right). The dotted contours represent negative values.

desired limit, i.e. $48° \pm 4°$, the Reynolds number has to be higher than 520. It then can be concluded that the swirler has to be adapted to the Reynolds number range.

It is then possible to compute the mass-flow-averaged swirling angle at any cross section downstream from the swirler and to plot its evolution. Fig. 16 clearly shows the dependency of this evolution with the Reynolds number. For highly viscous fluids ($Re \approx 50$), friction forces are so large that the swirl vanishes within seven diameters.

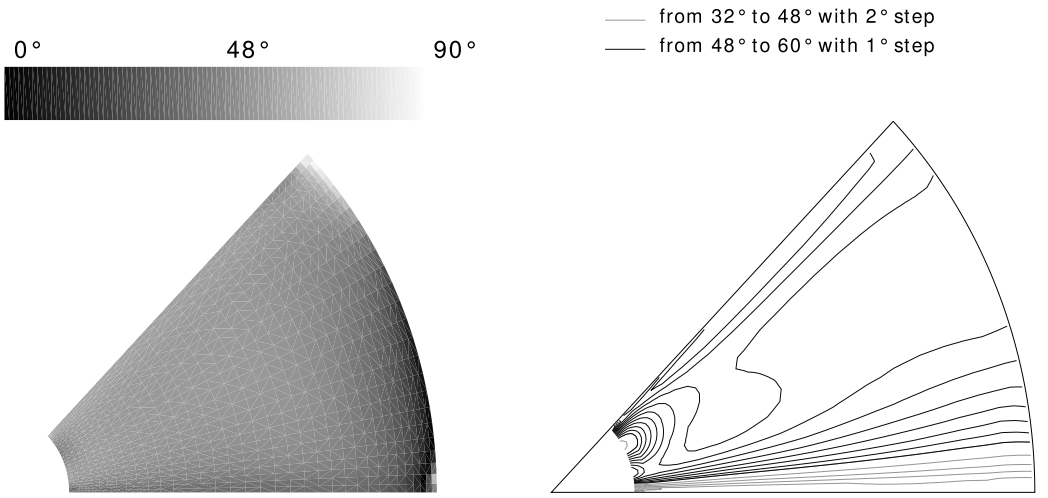

Fig. 13. Flow exit angle at the outlet of the swirler blades ($z/D = 0$) for $Re = 1600$.

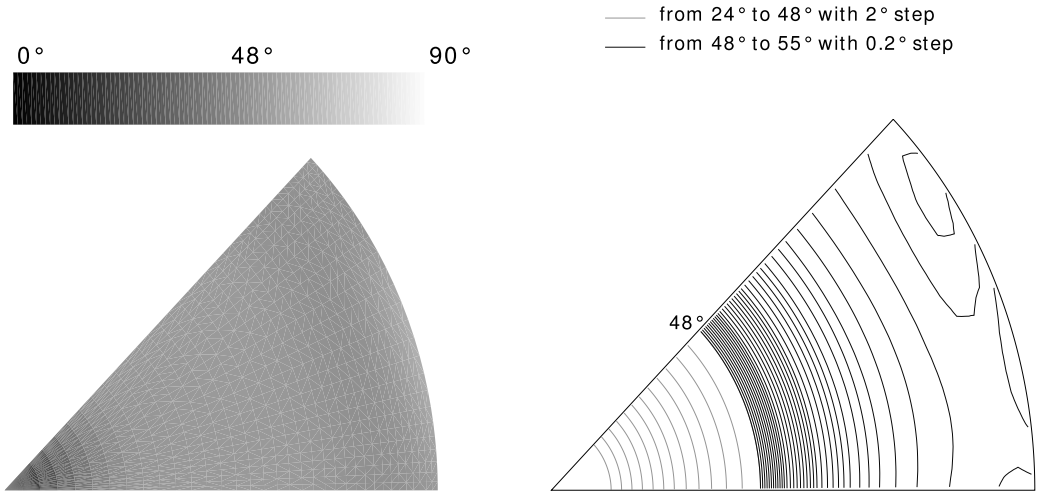

Fig. 14. Swirling angle for $Re = 1600$ at $z/D = 1$.

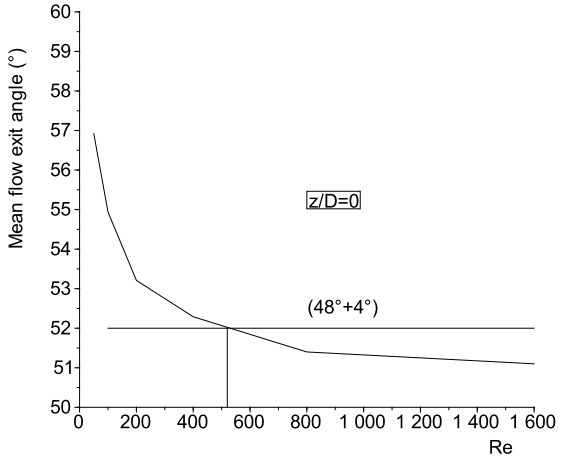

Fig. 15. Mean flow exit angle at the outlet of the swirler.

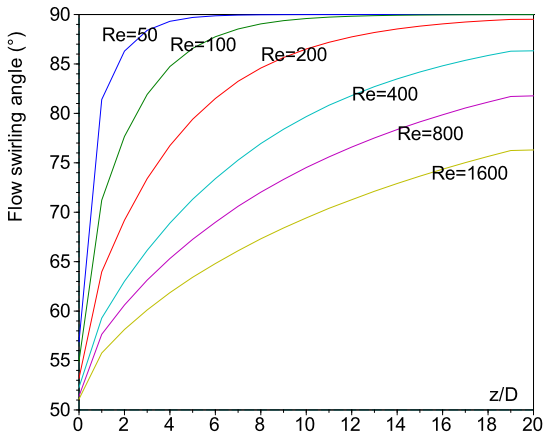

Fig. 16. Mean swirling angle.

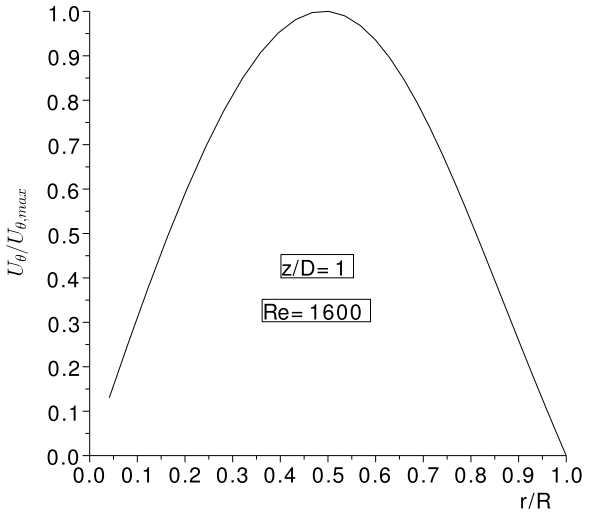

Fig. 17. Radial profile of the tangential velocity at $z/D = 1$.

A notable characteristic of the swirl is the radial distribution of the tangential velocity. Fig. 17 shows as an example the reduced velocity profile at $z/D = 1$. It must be noted that in the studied range of Reynolds numbers, the location of the maximum tangential velocity varies by less than 10% of the radius.

Then it is possible to plot the evolution of $U_{\theta,\max}/(U_{\theta,\max})_{z/D=1}$ versus z/D (Fig. 18) as a function of the Reynolds number. It is found that it is possible to approximate the values using the following equations:

$$\frac{U_{\theta,\max}}{(U_{\theta,\max})_{z/D=1}} = \exp\left(-\alpha\left[\frac{z}{D} - 1\right]\right)$$

$$\alpha = \frac{\sigma}{Re} + \mu$$

with the dimensionless parameters $\sigma = 41 \pm 0.1$ and $\mu = 0.0174 \pm 0.0001$.

4. Conclusion

This paper has presented the design process of a swirler, and it has been shown that the main goal is achieved, i.e. the fluid deviates by an angle which is within a given design range, for a quite large range of the Reynolds number (520 to 1600).

It has been shown that it is possible to approximate the evolution of the maximum tangential velocity, knowing that the radial distribution is self similar at any downstream axial location.

A test rig will soon be available at the “Université de Valenciennes et du Hainaut-Cambrésis”. It will then be possible to compare the experimental data to the computed values. A particular effort will be made in a comparison of the wall shear stress distributions, as the final goal is to increase the convection heat transfer coefficient.

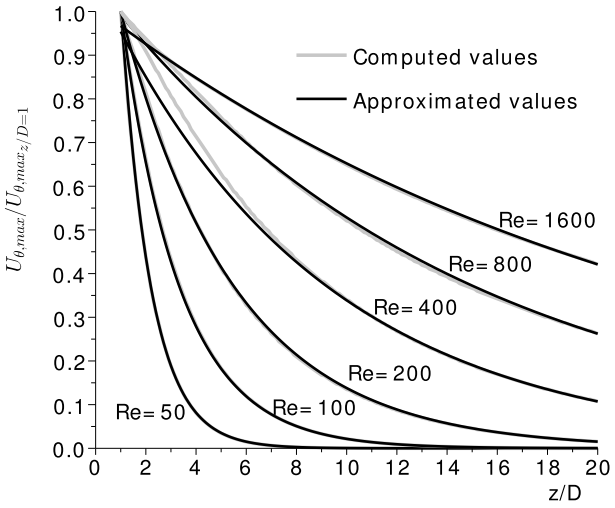

Fig. 18. Maximum tangential velocity.

Acknowledgements

The authors are grateful to the "Université de Valenciennes et du Hainaut-Cambrésis" for the financial support of the "FISF" project (Fundamentals of Internal Swirling Flows), Grant # 915POLETD-C915PRPT-ARI-FISF and to Prof. Desmet and Prof. Monnoyer for the very fruitful discussions on the physics of swirling flows, and for the very useful advices on the use of the CFD code.

The authors would finally want to thank the reviewers for informative comments and advice that did improve the paper markedly.

References

[1] www.engr.iupui.edu/me/courses/shellandtube.
[2] A.F. Najafi, S.M. Mousavian, K. Amini, Numerical investigations on swirl intensity decay rate for turbulent swirling flow in a fixed pipe, Int. J. Mech. Sci. 53 (2011) 801–811.
[3] A. Escue, J. Cui, Comparison of turbulence models in simulating swirling pipe flows, Appl. Math. Model. 34 (10) (2010) 2840–2849.
[4] K.M. Saqr, et al., Computational study of decaying annular vortex flow using the $Re_\varepsilon/\kappa - \varepsilon$ turbulence model, Appl. Math. Model. 36 (10) (2011) 4652–4664.
[5] A.F. Ryzhkov, L. Zhargalkhuu, Nadir Saman, M. Sharif, A.D. Makhaev, Estimation of the thermohydraulic efficiency of swirlers at small Reynolds numbers, J. Eng. Phys. Thermophys. 82 (1) (2009) 21–28.
[6] A.M. Jawarneh, G.H. Vatistas, A. Ababneh, Analytical approximate solution for decaying laminar swirling flows within a narrow annulus, Jordan J. Mech. Ind. Eng. 2 (2) (2008) 101–109.
[7] T.F. Ayinde, A generalized relationship for swirl decay in laminar pipe flow, Sâdhana 35 (2) (2010) 129–137.
[8] S.K. Saha, A. Dutta, S.K. Dhal, Friction and heat transfer characteristics of laminar swirl flow through a circular tube fitted with regularly spaces twisted-tape elements, Int. J. Heat Mass Transf. 44 (2001) 4211–4223.
[9] K. Wongcharee, S. Eiamsa-ard, Friction and heat transfer characteristics of laminar swirl flow through the round tubes inserted with alternate clockwise and counter-clockwise twisted-tapes, Int. Commun. Heat Mass Transf. 38 (3) (2011) 348–352.
[10] Radu Cazan, Cyrus K. Aidun, Experimental investigation of the swirling flow and the helical vortices induced by a twisted tape inside a circular pipe, Phys. Fluids 21 (2009) 037102.
[11] P. Promvonge, S. Pethkool, M. Pimsarn, C. Thianpong, Heat transfer augmentation in a helical-ribbed tube with double twisted tape inserts, Int. Commun. Heat Mass Transf. 39 (2012) 953–959.
[12] S. Woei, C. Ming, H. Guo, Thermal performances of enhanced smooth and spiky twisted tapes for laminar and turbulent tubular flows, Int. J. Heat Mass Transf. 55 (2012) 7651–7667.
[13] T. Sherman Pottebaum, M. Gharib, Using oscillations to enhance heat transfer for a circular cylinder, Int. J. Heat Mass Transf. 49 (2006) 3190–3210.
[14] S. Martemianov, V.L. Okulov, On heat transfer enhancement in swirl pipe flows, Int. J. Heat Mass Transf. 47 (2004) 2379–2393.
[15] F. Chang, V.K. Dhir, Mechanisms of heat transfer enhancement and slow decay of swirl in tubes using tangential injection, Int. J. Heat Fluid Flow 16 (1995) 78–87.
[16] J. Wang, G.H. Priestman, J.R. Tippetts, Modelling of strongly swirling flows in a complex geometry using unstructured meshes, Int. J. Numer. Methods Heat Fluid Flow 16 (8) (2006) 910–926.
[17] M. Yilmaz, O. Comakli, S. Yapici, O. Nuri Sara, Heat transfer and friction characteristics in decaying swirl flow generated by different radial guide vane swirl generators, Energy Convers. Manag. 44 (2003) 283–300.
[18] S. Eiamsa-ard, S. Rattanawong, P. Promvonge, Turbulent convection in round tube equipped with propeller type swirl generators, Int. Commun. Heat Mass Transf. 36 (2009) 357–364.
[19] İ. Kurtbaş, F. Gülçimen, A. Akbulut, D. Buran, Heat transfer augmentation by swirl generators inserted into a tube with constant heat flux, Int. Commun. Heat Mass Transf. 36 (2009) 865–871.
[20] R. Rey, R. Noguera, Profils, grilles d'aubes et machines axiales, Arts et Métiers ParisTech, available at www.lemfi.eu/activites/cours/cours_en_ligne/cours_rey_2_TOMEII.pdf, November 2008.
[21] P. Hill, C. Peterson, Mechanics and Thermodynamics of Propulsion, second edition, Addison-Wesley Publishing Company, ISBN 0-201-14659-2, 1992.

[22] R.A. Wallis, A rationalised approach to blade element design, axial flow fans, in: Proceedings of the Conference on Hydraulics and Fluid Mechanics, paper #2599, Sydney, Australia, 25–29 November, 1968.
[23] C. Bak, P. Fuglsang, N.N. Sørensen, H.A. Madsen, W.Z. Shen, J.N. Sørensen, Airfoil characteristics for wind turbines, Risø-R-1065(EN), Risø National Laboratory, Roskilde, Denmark, March 1999.
[24] D. Salomon, Curves and Surfaces for Computer Graphic, Springer-Verlag, 2005.
[25] H.G. Weller, G. Tabor, H. Jasak, C. Fureby, A tensorial approach to computational continuum mechanics using object orientated techniques, Comput. Phys. 12 (6) (1998) 620–631.
[26] http://www.openfoam.org/.
[27] H.K. Versteeg, W. Malalasekera, An Introduction to Computational Fluid Dynamics: The Finite Volume Method, 2nd edition, Pearson Prentice Hall, ISBN 9780131274983, 2007.
[28] S.V. Patankar, Numerical Heat Transfer and Fluid Flow, Ser. Comput. Methods Mech. Therm. Sci., Taylor & Francis, ISBN 0-89116-522-3, 1980.
[29] K.S. Shterev, S.K. Stefanov, Pressure-based finite volume method for calculation of compressible gas flows, J. Comput. Phys. 229 (2010) 461–480.
[30] http://www.scilab.org/.